Available online at www.sciencedirect.com
ScienceDirect
Journal of Catalysis 254 (2008) 198–204
JOURNAL OF CATALYSIS
www.elsevier.com/locate/jcat

Effect of post-calcination on photocatalytic activity of $(Ga_{1-x}Zn_x)(N_{1-x}O_x)$ solid solution for overall water splitting under visible light

Kazuhiko Maeda [1], Kentaro Teramura [2], Kazunari Domen *

Department of Chemical System Engineering, The University of Tokyo, 7-3-1 Hongo, Bunkyo-ku, Tokyo 113-8656, Japan

Received 30 October 2007; revised 11 December 2007; accepted 15 December 2007

Available online 28 January 2008

Abstract

Post-calcination at moderate temperature is found to be effective for improving the activity of $(Ga_{1-x}Zn_x)(N_{1-x}O_x)$ as a photocatalyst for overall water splitting under visible light. The activity of $(Ga_{1-x}Zn_x)(N_{1-x}O_x)$ with a composition of $x = 0.12$ increases with post-calcination temperature up to 873 K, above which the material commences to decompose oxidatively. This activity enhancement is attributed to a reduction in the density of zinc- and/or oxygen-related defects that function as recombination centers for photogenerated electrons and holes. The degree of enhancement by post-calcination decreases with increasing ZnO composition (x), reflecting a decrease in the as-prepared defect density with increasing x. The optimized photocatalyst, with a composition of $x = 0.18$, loaded with $Rh_{2-y}Cr_yO_3$ cocatalyst (2.5 wt% Rh, 2 wt% Cr) and post-calcined at 823 K, exhibits an apparent quantum efficiency of ca. 5.9% at 420–440 nm, which is more than two times higher than that of the previously reported catalyst (ca. 2.5% at 420–440 nm).

Keywords: Heterogeneous photocatalysis; Hydrogen production; Light energy conversion; Overall water splitting; Post-treatment; Visible light

1. Introduction

The key to producing highly active heterogeneous photocatalysts is to suppress recombination of photogenerated electrons and holes so as to maximize the number of photogenerated carriers that can participate in surface chemical reactions [1–4]. Increasing the crystallinity of the material generally enhances activity by reducing the density of defects, which act as recombination centers. Thus, refining the preparation conditions so as to obtain a photocatalyst with high crystallinity is generally an effective strategy for improving photocatalytic performance. It is also known, however, that the photocatalytic activity of a given material can be improved by applying appropriate post-treatment [5–9]. For example, high-pressure treatment of Ta_3N_5 and Ge_3N_4 by exposure to NH_3 gas has been demonstrated to reduce the defect density and thereby improve the photocatalytic activity of these materials for H_2 evolution from aqueous methanol solution (Ta_3N_5) and for overall water splitting (Ge_3N_4) [5,6]. Kominami et al. reported that nanocrystalline TiO_2 prepared by hydrothermal crystallization in organic media (HyCOM) exhibits greater activity for certain photocatalytic reactions (such as H_2 evolution from aqueous 2-propanol solution and O_2 evolution from aqueous silver sulfate solution) upon post-calcination in air; this increase in activity is due to a reduction in the recombination probability between photogenerated electrons and holes [7,8]. It has also been reported by Sayama et al. that H_2-reduction and subsequent O_2-oxidation of $K_4Nb_6O_{17}$ leads to an improvement in overall water splitting activity, although the reason for this enhanced activity was not clarified [9].

In heterogeneous photocatalysis, overall water splitting under visible light is acknowledged to be one of the most important and valuable photocatalytic reactions since it is a potential means of producing clean and renewable hydrogen fuel from solar energy and water [2–4]. Our research group has been developing nonoxide photocatalysts that are active for this reac-

* Corresponding author. Fax: +81 3 5841 8838.
E-mail address: domen@chemsys.t.u-tokyo.ac.jp (K. Domen).
[1] Research Fellow of the Japan Society for the Promotion of Science (JSPS).
[2] Present address: Pioneering Research Unit for Next Generation, Kyoto University.

0021-9517/$ – see front matter
doi:10.1016/j.jcat.2007.12.009

Table 1
Preparation conditions for $(Ga_{1-x}Zn_x)(N_{1-x}O_x)$

x in $(Ga_{1-x}Zn_x)(N_{1-x}O_x)$	Amount of starting materials (g)		Nitridation conditions	
	β-Ga_2O_3	ZnO	Temperature (K)	Time (h)
0.12	1.08	0.94	1123	15
0.18	0.73	1.27	1123	10
0.23	1.08	0.94	1223	1.5

tion [4], the most promising example of which is the solid solution of GaN and ZnO (represented as $(Ga_{1-x}Zn_x)(N_{1-x}O_x)$) [10–19]. The catalytic activity of $(Ga_{1-x}Zn_x)(N_{1-x}O_x)$ has been systematically improved by optimizing the preparation conditions [11,12], identifying cocatalysts that efficiently promote the reaction [13–17], and clarifying suitable reaction conditions [18]. Through these efforts, the apparent quantum efficiency of the $(Ga_{1-x}Zn_x)(N_{1-x}O_x)$ system has been increased to ca. 2.5% at 420–440 nm. However, there still appears to be substantial room for improving the activity of this catalyst by considering post-preparation treatments [13].

In the present study, the effect of post-calcination on the activity of $(Ga_{1-x}Zn_x)(N_{1-x}O_x)$ for visible-light-driven overall water splitting is investigated by conducting a detailed structural and physicochemical analysis.

2. Experimental

2.1. Materials

$(Ga_{1-x}Zn_x)(N_{1-x}O_x)$ solid solutions were prepared by heating a mixture of β-Ga_2O_3 and ZnO powders (ca. 2 g) under NH_3 flow (250 ml min^{-1}) according to the method described previously [10,11]. Detailed preparation conditions are summarized in Table 1. After nitridation, the sample was cooled to room temperature under NH_3 flow. The production of $(Ga_{1-x}Zn_x)(N_{1-x}O_x)$ with $x = 0.12$, 0.18, and 0.23 was confirmed by powder X-ray diffraction (XRD) and energy-dispersive X-ray analysis (EDX). The as-synthesized $(Ga_{1-x}Zn_x)(N_{1-x}O_x)$ powder was then subjected to post-calcination in a static air atmosphere at 573–1173 K for 1 h.

GaN and $ZnGa_2O_4$ were used as references. GaN was purchased from Mitsubishi Chemicals Co., while $ZnGa_2O_4$ was prepared by heating a stoichiometric mixture of β-Ga_2O_3 and ZnO powders at 1273 K for 16 h in air. The production of $ZnGa_2O_4$ was confirmed by XRD analysis and EDX spectroscopy.

2.2. Modification with nanoparticulate $Rh_{2-y}Cr_yO_3$

Nanoparticulate Rh–Cr mixed-oxide ($Rh_{2-y}Cr_yO_3$), a cocatalyst assisting H_2 evolution, was loaded onto the as-prepared $(Ga_{1-x}Zn_x)(N_{1-x}O_x)$ catalyst according to the method described previously [10–13]. Briefly, 0.3–0.4 g of $(Ga_{1-x}Zn_x)(N_{1-x}O_x)$ powder and 3–4 ml of distilled water containing an appropriate amount of $Na_3RhCl_6{\cdot}2H_2O$ and $Cr(NO_3)_3{\cdot}9H_2O$ were placed in an evaporating dish over a water bath. The suspension was stirred using a glass rod to complete evaporation. The resulting powder was collected and heated in air at 623 K for 1 h to convert Rh and Cr species to $Rh_{2-y}Cr_yO_3$ [15].

2.3. Characterization of catalysts

The prepared samples were studied by powder XRD (RINT-UltimaIII, Rigaku; Cu$K\alpha$), thermogravimetry (TG; DTG-50, Shimadzu), scanning electron microscopy (SEM; S-4700, Hitachi), EDX (Emax-7000, Horiba), X-ray photoelectron spectroscopy (XPS; Shimadzu ESCA-3200), X-ray absorption fine-structure (XAFS) spectroscopy, ultraviolet–visible diffuse reflectance spectroscopy (DRS; V-560, Jasco), and photoluminescence (PL) spectroscopy (FP-6600, Jasco). TG analysis was performed under a flow of air (50 ml min^{-1}) at a heating rate of 10 K min^{-1}. The PL spectra were measured at room temperature under excitation at 420 nm provided by emission from a xenon lamp. XAFS measurements of Ga– and Zn–K edge spectra were performed at the BL01B1 beamline of the SPring-8 synchrotron facility (Hyogo, Japan) using a ring energy of 8 GeV and a stored current of 100 mA in top-up mode (Proposal No. 2007A1803). XAFS spectra were measured in transmission mode at room temperature using an Si(111) two-crystal monochromator. Data reduction was performed using the REX2000 program (Rigaku). The photon energies in X-ray absorption near-edge structure (XANES) spectra were corrected in reference to Cu foil (8980.3 eV) for Ga–K edge spectra and Zn foil (9659 eV) for Zn–K edge spectra. The Brunauer–Emmett–Teller (BET) surface area was measured using a BELSORP-mini instrument (BEL Japan) at liquid nitrogen temperature.

2.4. Photocatalytic reactions

Photocatalytic reactions were carried out in a Pyrex inner-irradiation reaction vessel connected to a glass closed gas circulation system. A 0.3 g sample of the $Rh_{2-y}Cr_yO_3$-loaded catalyst powder was dispersed in an aqueous H_2SO_4 solution (370 ml) adjusted to pH 4.5. The peak catalytic performance of this material for overall water splitting was previously shown to occur at pH 4.5 [18]. The reactant solution was first evacuated several times to ensure complete air removal. It was then irradiated under a 450 W high-pressure mercury lamp via a Pyrex tube filled with aqueous $NaNO_2$ solution (2 M) that acted as a filter to block ultraviolet (UV) light, thereby ensuring irradiation only at wavelengths longer than 400 nm [10–18]. The reactant solution was maintained at room temperature by a flow of cooling water during the reaction. The evolved gases were analyzed by gas chromatography.

The quantum efficiency (Φ) was estimated by the method described previously [13] using the equation

$$\Phi(\%) = (2 \times H/I) \times 100, \quad (1)$$

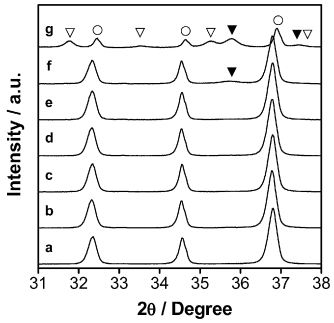

Fig. 1. Powder XRD patterns of $(Ga_{1-x}Zn_x)(N_{1-x}O_x)$ ($x = 0.12$) (a) as-prepared and (b–g) after calcination in air for 1 h at (b) 573, (c) 773, (d) 873, (e) 973, (f) 1073, and (g) 1173 K. Open triangles denote diffractions assigned to β-Ga_2O_3, solid triangles denote $ZnGa_2O_4$, and open circles denote GaN.

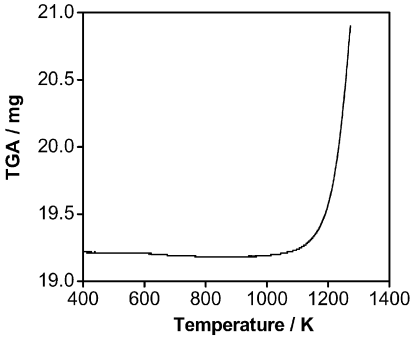

Fig. 2. Thermogravimetry result for as-prepared $(Ga_{1-x}Zn_x)(N_{1-x}O_x)$ ($x = 0.12$) obtained at a heating rate of 10 K min^{-1} under air (50 ml min^{-1}).

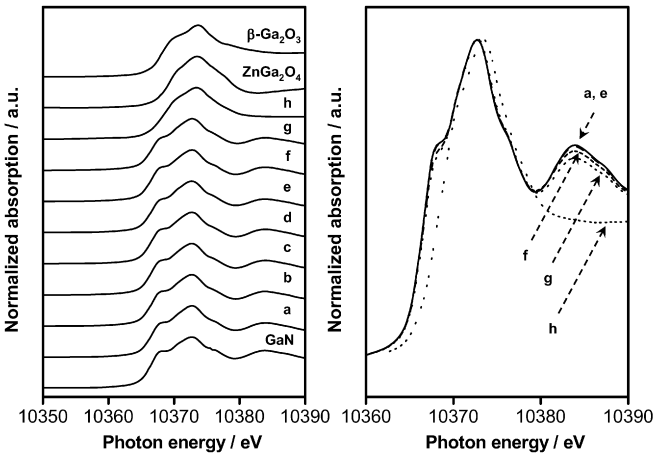

Fig. 3. Ga–K edge XANES spectra for $(Ga_{1-x}Zn_x)(N_{1-x}O_x)$ ($x = 0.12$) (a) as-prepared and (b–h) after calcination in air for 1 h at (b) 573, (c) 673, (d) 773, (e) 873, (f) 973, (g) 1073, and (h) 1173 K. The spectra on the left are overlaid above each other, whereas those on the right are superimposed on top of each other. Spectra for GaN, $ZnGa_2O_4$, and β-Ga_2O_3 are shown for reference.

where H and I represent the numbers of evolved H_2 molecules and incident photons, respectively. It is assumed that all incident photons are absorbed by the photocatalyst. A Pyrex top-irradiation reaction vessel and a 300 W xenon lamp fitted with a cutoff filter were employed for quantum efficiency measurements. The number of incident photons was measured using a calibrated Si photodiode.

3. Results and discussion

3.1. Structural properties

Fig. 1 shows the XRD patterns of $(Ga_{1-x}Zn_x)(N_{1-x}O_x)$ ($x = 0.12$) calcined at various temperatures. All samples calcined at temperatures lower than 973 K exhibit single-phase diffraction patterns indicative of a hexagonal wurtzite structure similar to GaN and ZnO [10,11]. At 1073 K, however, a small diffraction peak, assignable to $ZnGa_2O_4$, appears at ca. $2\theta = 35.8°$ accompanied by a slight decrease in diffraction peak intensities (line f). Calcination at 1173 K results in disappearance of the peaks attributable to $(Ga_{1-x}Zn_x)(N_{1-x}O_x)$ and emergence of new diffraction peaks assigned to β-Ga_2O_3 and GaN, accompanied by a strengthening of the $ZnGa_2O_4$ peak (line g). These results indicate that the crystal structure of $(Ga_{1-x}Zn_x)(N_{1-x}O_x)$ ($x = 0.12$) is retained at calcination temperatures of up to 973 K, and that decomposition of the crystal structure begins to take place when calcined at temperatures higher than 1073 K. This change in crystal structure agrees with the result of TG analysis (Fig. 2), which shows that the sample weight remained almost unchanged at temperatures lower than 1023 K but increased markedly with increasing temperature from 1023 K due to the replacement of nitrogen with oxygen in the material. The lack of change in the intensity and position of diffraction peak for samples post-calcined below 973 K also indicates that samples thus treated do not undergo particle growth or compositional change. It was confirmed by SEM that the samples post-calcined at temperatures below 973 K exhibit very little difference from the as-prepared samples, with unchanged specific surface areas and Zn/Ga atomic ratios as determined by EDX analyses. In addition, XPS analyses revealed that the surface atomic composition (N/Ga) of $(Ga_{1-x}Zn_x)(N_{1-x}O_x)$ ($x = 0.12$) remains unchanged even upon post-calcination up to 873 K, indicating that no surface oxidation takes place. This result is supported by the data for TG analysis.

The local structure and valence state of gallium and zinc in the samples calcined at various temperatures were investigated by XAFS measurements. Fig. 3 shows Ga–K edge XANES spectra for $(Ga_{1-x}Zn_x)(N_{1-x}O_x)$ ($x = 0.12$) after post-calcination at various temperatures. The data for GaN, $ZnGa_2O_4$, and β-Ga_2O_3 are shown for comparison. The Ga–K edge spectrum for the as-prepared sample is identical to that for GaN, indicating that the local structure and valence state of gallium atoms in $(Ga_{1-x}Zn_x)(N_{1-x}O_x)$ ($x = 0.12$) is close to that in GaN. This result is also supported by a previous X-ray photoelectron spectroscopy (XPS) study, which revealed that the valence state of gallium in $(Ga_{1-x}Zn_x)(N_{1-x}O_x)$ is similar to that in GaN [11]. Upon post-calcination at temperatures lower than 873 K, the spectral shape and the absorption edge of samples remained unchanged (spectra a–e); this indicates that post-calcination below 873 K has little effect on the local structure or valence state of gallium in $(Ga_{1-x}Zn_x)(N_{1-x}O_x)$ ($x = 0.12$). However, the spectral shape begins to change for samples treated at 973 K (spectrum f) or above, eventually affording the characteristic spectral shapes around 10368 and

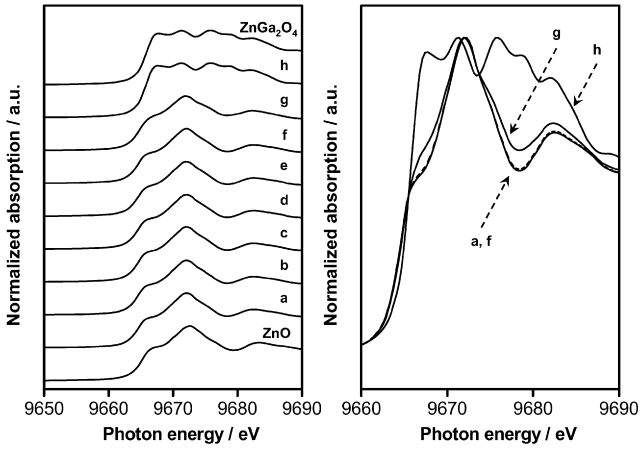

Fig. 4. Zn–K edge XANES spectra for $(Ga_{1-x}Zn_x)(N_{1-x}O_x)$ ($x = 0.12$) (a) as-prepared and (b–h) after calcination in air for 1 h at (b) 573, (c) 673, (d) 773, (e) 873, (f) 973, (g) 1073, and (h) 1173 K. The spectra on the left are overlaid above each other, whereas those on the right are superimposed on top of each other. Spectra for ZnO, and $ZnGa_2O_4$ are shown for reference.

10384 eV in samples calcined at 1173 K. This change is accompanied by a shift of the absorption edge to higher photon energies. The spectrum for the 1173 K sample is similar to the spectra for the $ZnGa_2O_4$ and β-Ga_2O_3 references, indicating that the GaN-like structure of $(Ga_{1-x}Zn_x)(N_{1-x}O_x)$ collapses completely upon calcination at 1173 K, in good agreement with the results of XRD measurements (Fig. 1).

Fig. 4 shows the Zn–K edge XANES spectra for the same samples, along with ZnO and $ZnGa_2O_4$ data for comparison. The variation of the Zn–K edge spectra exhibits a similar tendency to the variation of the Ga–K edge spectra. The Zn–K edge spectrum for the as-prepared sample is identical to that for ZnO, although the absorption edge of the former appears at slightly lower photon energies than for the latter. The slight shift in photon energy is attributable to the difference in bonding polarity between Zn–N and Zn–O; that is, Zn–N bonding is more covalent than Zn–O bonding, suggesting that Zn–N bonding is formed in this material. This result is consistent with previous XPS results [11]. The spectral shape of the as-prepared sample underwent little change upon post-calcination at temperatures lower than 973 K, indicating no change in the local structure and valence state of zinc. The XANES spectrum for the 1073 K sample exhibits slight differences from the XANES spectra for samples calcined at temperatures lower than 973 K. In contrast, the XANES spectrum for the 1173 K sample differs distinctly from the spectra for samples calcined at temperatures lower than 973 K, and it is identical to that for the $ZnGa_2O_4$ reference. These results indicate that the structure in the vicinity of zinc and the valence state of zinc in $(Ga_{1-x}Zn_x)(N_{1-x}O_x)$ ($x = 0.12$) remain unchanged when calcined at 973 K or below, but that they begin to change from 1073 K. The results obtained by XAFS measurements are thus in good agreement with the results obtained by XRD (Fig. 1).

The above characterization reveals that the structural characteristics of $(Ga_{1-x}Zn_x)(N_{1-x}O_x)$ ($x = 0.12$) remain almost unchanged upon post-calcination at temperatures of 873 K or below. Calcination at temperatures of 973 K or higher, however, causes changes to the material and at a sufficiently high temperature (i.e., 1173 K) causes complete oxidative decomposition.

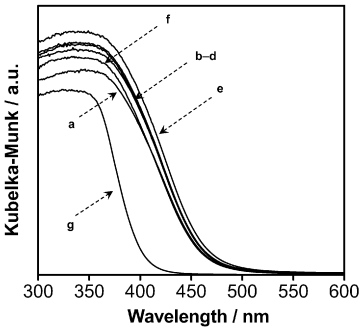

Fig. 5. UV–visible diffuse reflectance spectra for $(Ga_{1-x}Zn_x)(N_{1-x}O_x)$ ($x = 0.12$) (a) as-prepared and (b–g) after calcination in air for 1 h at (b) 573, (c) 773, (d) 873, (e) 973, (f) 1073, and (g) 1173 K.

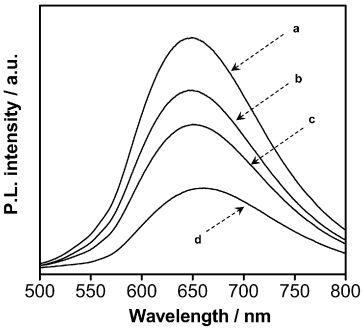

Fig. 6. Photoluminescence spectra measured at room temperature for $(Ga_{1-x}Zn_x)(N_{1-x}O_x)$ ($x = 0.12$) (a) as-prepared and (b–d) calcined in air for 1 h at (b) 573, (c) 773, and (d) 873 K. Excitation wavelength, 420 nm.

3.2. Optical properties

The UV–visible diffuse reflectance spectra for samples calcined at various temperatures are shown in Fig. 5. The as-prepared $(Ga_{1-x}Zn_x)(N_{1-x}O_x)$ ($x = 0.12$) displays an absorption edge at around 470 nm (spectrum a). Post-calcination up to 973 K slightly shifts the absorption edge to longer wavelengths (spectra b–e), whereas treatment at higher temperatures causes a blue shift (spectrum f) toward ca. 400 nm upon calcination at 1173 K (spectrum g). Although the origin of the slight red-shift in the absorption edge is not clear at present, the significant blue-shift in absorption edge after post-calcination at 1173 K is attributable to the collapse of the $(Ga_{1-x}Zn_x)(N_{1-x}O_x)$ ($x = 0.12$) structure.

As demonstrated in a previous study, as-prepared $(Ga_{1-x}Zn_x)(N_{1-x}O_x)$ exhibits PL resulting from the recombination of photogenerated electrons and holes [19]. The PL process is largely governed by the presence of surface vacancies and defects since they act as recombination centers for photogenerated electrons and holes. The number of these surface vacancies and defects can be modified by post-preparation treatment [6,20]. Fig. 6 shows the PL spectra for $(Ga_{1-x}Zn_x)(N_{1-x}O_x)$ calcined at various temperatures. All samples exhibit a PL band at around 650 nm upon photoex-

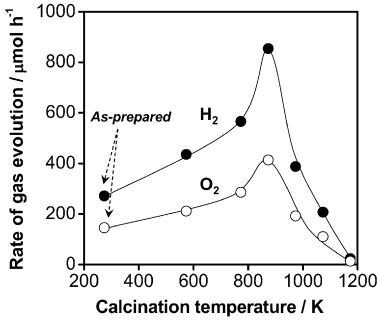

Fig. 7. Dependence of steady rate of H_2 and O_2 evolution in overall water splitting under visible light ($\lambda > 400$ nm) on post-calcination temperature of $(Ga_{1-x}Zn_x)(N_{1-x}O_x)$ ($x = 0.12$). Reaction conditions: catalyst, 0.3 g; cocatalyst, $Rh_{2-y}Cr_yO_3$ (1 wt% Rh, 1.5 wt% Cr); reaction solution, aqueous H_2SO_4 solution adjusted to pH 4.5 (370 ml); light source, high-pressure mercury lamp (450 W); reaction vessel, Pyrex inner-irradiation vessel with aqueous $NaNO_2$ solution filter.

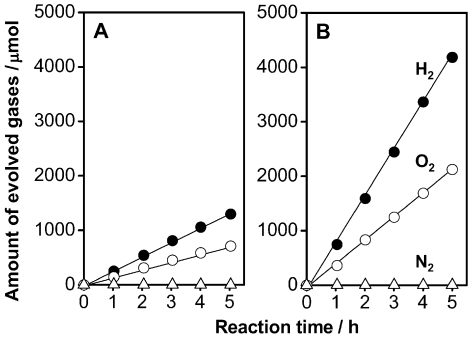

Fig. 8. Time courses of overall water splitting under visible light ($\lambda > 400$ nm) for $(Ga_{1-x}Zn_x)(N_{1-x}O_x)$ ($x = 0.12$) (A) before and (B) after post-calcination in air at 873 K for 1 h. Reaction conditions: catalyst, 0.3 g; cocatalyst, $Rh_{2-y}Cr_yO_3$ (1 wt% Rh, 1.5 wt% Cr); reaction solution, aqueous H_2SO_4 solution adjusted to pH 4.5 (370 ml); light source, high-pressure mercury lamp (450 W); reaction vessel, Pyrex inner-irradiation vessel with aqueous $NaNO_2$ solution filter.

citation at 420 nm, with the peak position shifting slightly to longer wavelengths with increasing post-calcination temperature. However, the intensity of the PL band also decreases markedly with increasing post-calcination temperature. This result indicates that post-calcination of $(Ga_{1-x}Zn_x)(N_{1-x}O_x)$ reduces the density of photogenerated carrier traps in the material and is thus expected to promote photocatalytic activity.

3.3. Photocatalytic activity

Fig. 7 shows the dependence of the steady rate of H_2 and O_2 evolution in overall water splitting under visible light ($\lambda > 400$ nm) on post-calcination temperature for $(Ga_{1-x}Zn_x)(N_{1-x}O_x)$ ($x = 0.12$). All catalysts produced H_2 and O_2 stoichiometrically. The experimental error in the rates of H_2 and O_2 evolution was within 10%. However, the rates of H_2 and O_2 evolution increased with calcination temperature to a maximum at 873 K, beyond which the activity of the samples began to decrease significantly. Fig. 8 shows the time courses of overall water splitting under visible light on the as-prepared catalyst (loaded with $Rh_{2-y}Cr_yO_3$) and the same material after calcination at 873 K. Both catalysts produced H_2 and O_2 steadily and stoichiometrically, and the amount of evolved gases increased with reaction time. However, the activity of the calcined sample was three times higher than that of the as-prepared sample. The total H_2 and O_2 evolution over 5 h of reaction (6.3 mmol) using the calcined sample was substantially greater than the amount of catalyst employed (3.7 mmol), providing confirmation of the catalytic cycle. A low level of N_2 evolution (ca. 5 μmol) was detected in the initial stage of the reaction (first 1–2 h) for both of these catalysts, attributable to the oxidation of N^{3-} species near the $(Ga_{1-x}Zn_x)(N_{1-x}O_x)$ surface to N_2 [18]. However, the production of N_2 disappears completely as the reaction progresses, and no changes in the XRD pattern of the catalyst were detected as a result of the reaction. These results clearly indicate that post-calcination is highly effective for enhancing the photocatalytic activity of $(Ga_{1-x}Zn_x)(N_{1-x}O_x)$ for overall water splitting under visible light.

The enhanced activity of $(Ga_{1-x}Zn_x)(N_{1-x}O_x)$ with increasing post-calcination temperature is considered to reflect a reduction in the probability of recombination between photogenerated carriers due to a reduction in the defect density in the material. This effect appears to be at least partially correlated with the results of PL measurements (Fig. 6). For samples post-calcined at temperatures up to 873 K (the greatest increase in activity increase was obtained at 873 K), the intensity of the PL band decreases considerably in association with the reduction in the density of defects, which act as recombination centers; this is despite the fact that samples post-calcined at temperatures lower than 873 K display no appreciable change in structure properties. Post-calcination at temperatures higher than 973 K, on the other hand, results in structural collapse, exemplified by the change in the local structure around zinc atoms to form a $ZnGa_2O_4$-like structure. At sufficiently high temperature, the wurtzite structure of $(Ga_{1-x}Zn_x)(N_{1-x}O_x)$ is decomposed. This structural decomposition is considered to be the main reason for the decrease in activity at higher calcination temperatures.

3.4. Effect of composition on the effectiveness of post-calcination

The dependence of the activity improvement achieved by post-calcination on the composition of the $(Ga_{1-x}Zn_x)(N_{1-x}O_x)$ solid solution was investigated using the optimum post-calcination condition of 873 K. The photocatalytic activities for overall water splitting achieved using as-prepared and post-calcined samples with compositions of $x = 0.12, 0.18$, and 0.23 are listed in Table 2. Reactions were performed under visible light ($\lambda > 400$ nm). The enhancement ratio E presented in the table is defined by

$$E = \frac{\text{activity after post-calcination}}{\text{activity before post-calcination}}. \quad (2)$$

Although all samples achieved stoichiometric decomposition of water into H_2 and O_2 under visible light, E tended to decrease with increasing x from 0.12 to 0.23. This result indicates that post-calcination of $(Ga_{1-x}Zn_x)(N_{1-x}O_x)$ becomes less effective as the ZnO content (x) increases. This finding also implies

Table 2
Effect of post-calcination on photocatalytic activity of $(Ga_{1-x}Zn_x)(N_{1-x}O_x)$ for overall water splitting under visible light ($\lambda > 400$ nm)[a]

Entry	x in $(Ga_{1-x}Zn_x)(N_{1-x}O_x)$	Post-treatment[b]	Activity (μmol h^{-1})		E[c]	D_{PL}[d] (%)
			H_2	O_2		
1	0.12	No	270	134		
2		Yes	839	421	3.1	36
3	0.18	No	677	341		
4		Yes	927	460	1.4	64
5	0.23	No	183	86		
6		Yes	217	101	1.2	77

[a] Reaction conditions: catalyst, 0.3 g; cocatalyst, $Rh_{2-y}Cr_yO_3$ (1 wt% Rh, 1.5 wt% Cr); reaction solution, aqueous H_2SO_4 solution adjusted to pH 4.5 (370 ml); light source, high-pressure mercury lamp (450 W); reaction vessel, Pyrex inner-irradiation vessel with aqueous $NaNO_2$ solution filter.
[b] Calcination in air at 873 K for 1 h.
[c] Calculated using Eq. (2).
[d] Calculated using Eq. (3).

that the defect density in the as-prepared sample, which can be removed by post-calcination, decreases with increasing x.

Table 2 also presents the degree of decrease in the PL band around 650 nm. This change, denoted D_{PL}, is defined by

$$D_{PL}\ (\%) = \frac{\text{PL intensity after post-calcination}}{\text{PL intensity before post-calcination}} \times 100. \qquad (3)$$

The results indicate an increase in D_{PL} with increasing x. As the intensity of PL is related to the density of defects acting as traps of photogenerated carriers, the increase in D_{PL} with x indicates that as-prepared $(Ga_{1-x}Zn_x)(N_{1-x}O_x)$ with larger x values have a lower defect density that can be eliminated by post-calcination. As reported previously, $(Ga_{1-x}Zn_x)(N_{1-x}O_x)$ is typically obtained by nitriding a physical mixture of β-Ga_2O_3 and ZnO under a flow of NH_3 at temperatures higher than 1123 K, through which crystallization of $(Ga_{1-x}Zn_x)(N_{1-x}O_x)$ and reduction of ZnO in the material by H_2 (derived from disassociation of NH_3) take place simultaneously [11]. The reduction of ZnO in $(Ga_{1-x}Zn_x)(N_{1-x}O_x)$ introduces zinc- and/or oxygen-related vacancies in the crystal through the production of metallic zinc upon ZnO reduction. Metallic zinc is readily volatilized to afford zinc vapor, while the remaining oxygen species are removed as H_2O vapor. By this process, zinc and oxygen species in $(Ga_{1-x}Zn_x)(N_{1-x}O_x)$ are released from the surface rather than from the bulk [11]. It is therefore considered that the density of zinc- and/or oxygen-related defects in as-prepared $(Ga_{1-x}Zn_x)(N_{1-x}O_x)$ increases with decreasing x. This is supported by the decrease in the PL reduction realized by post-calcination with increasing x (Table 2).

On the basis of these results, it can be concluded that post-calcination eliminates zinc- and/or oxygen-related defects, which act as traps between photogenerated electrons and holes, thereby improving photocatalytic activity. However, post-calcination at excessively high temperatures results in destruction of the $(Ga_{1-x}Zn_x)(N_{1-x}O_x)$ structure and a corresponding degradation of activity. As post-calcination of GaN, a UV-active metal nitride photocatalyst [21], under the same conditions did not result in any increase in activity, it is considered that the present post-calcination treatment specifically affects the ZnO component of $(Ga_{1-x}Zn_x)(N_{1-x}O_x)$. Jing et al. claimed that surface defects in Zn-doped TiO_2 play an important role in promoting photocatalytic processes, thereby enhancing activity for phenol degradation [22]. However, Kominami et al. claimed that nanocrystalline TiO_2, which is prepared by HyCOM method, with less defect densities exhibits higher activity for certain photocatalytic reactions [8]. Accordingly, it is considered that whether defects have positive effect on activity or not is dependent on the kind of reactions and defects as well as the concentration of defects in a given photocatalyst, which appears to be complicated and can not be easily discussed. At least in the present case, it appears that surface defects related to Zn and/or O in $(Ga_{1-x}Zn_x)(N_{1-x}O_x)$ work as recombination centers between photogenerated electrons and holes in overall water splitting rather than offer active sites for the reaction. Since information on defects can be obtained not only by photoluminescence spectroscopy but also by another spectroscopic technique such as laser spectroscopy [23,24] and photoacoustic spectroscopy [25,26], the PL process and the state of surface defects in $(Ga_{1-x}Zn_x)(N_{1-x}O_x)$ will be investigated in more detail as part of future work by combination with such another technique.

3.5. Optimization of apparent quantum efficiency

The activity of the most promising $(Ga_{1-x}Zn_x)(N_{1-x}O_x)$ composition for overall water splitting from Table 2, $x = 0.18$, was finally maximized by optimizing the calcination temperature and cocatalyst loading rate. The maximum apparent quantum efficiency for overall water splitting, ca. 5.9% at 420–440 nm, was achieved by loading the photocatalyst with $Rh_{2-y}Cr_yO_3$ at a rate of 2.5 wt% Rh and 2 wt% Cr and calcining at 823 K. This apparent quantum efficiency is more than twice that of the previously reported catalyst (ca. 2.5% at 420–440 nm) [13], demonstrating the effectiveness of post-calcination at optimal temperature for improving photocatalytic activity by reducing the defect density in $(Ga_{1-x}Zn_x)(N_{1-x}O_x)$. However, it is considered that more than 90% of electron–hole pairs photogenerated in the material still undergo recombination without participating in overall water splitting. It is therefore expected that greater improvements in efficiency may be achieved by investigating alternative and complementary defect-reduction treatments for this material. Our research is now under way along this line.

4. Conclusion

The photocatalytic activity of $(Ga_{1-x}Zn_x)(N_{1-x}O_x)$ for overall water splitting under visible light was found to be improved by post-calcination treatment through reduction of the density of zinc- and/or oxygen-related defects in the material. The degree of activity improvement was found to be dependent on the calcination temperature and the composition of $(Ga_{1-x}Zn_x)(N_{1-x}O_x)$. The maximum quantum efficiency obtained by post-calcination treatment is ca. 5.9% at 420–440 nm.

Acknowledgments

This work was supported by the Research and Development in a New Interdisciplinary Field Based on Nanotechnology and Materials Science program of the Ministry of Education, Culture, Sports, Science and Technology (MEXT) of Japan. One of the authors (K.M.) is supported by a Fellowship from the Japan Society for the Promotion of Science (JSPS).

References

[1] M.R. Hoffmann, S.T. Martin, W. Choi, D.W. Bahnemann, Chem. Rev. 95 (1995) 69.
[2] A. Kudo, H. Kato, I. Tsuji, Chem. Lett. 33 (2004) 1534.
[3] J.S. Lee, Catal. Surv. Asia 9 (2005) 217.
[4] K. Maeda, K. Domen, J. Phys. Chem. C 111 (2007) 7851.
[5] Y. Lee, K. Nukumizu, T. Watanabe, T. Takata, M. Hara, M. Yoshimura, K. Domen, Chem. Lett. 35 (2006) 352.
[6] Y. Lee, T. Watanabe, T. Takata, M. Hara, M. Yoshimura, K. Domen, J. Phys. Chem. B 110 (2006) 17563.
[7] H. Kominami, S. Murakami, Y. Kera, B. Ohtani, Catal. Lett. 56 (1998) 125.
[8] H. Kominami, S. Murakami, J. Kato, Y. Kera, B. Ohtani, J. Phys. Chem. B 106 (2002) 10501.
[9] K. Sayama, H. Arakawa, K. Domen, Catal. Today 28 (1996) 175.
[10] K. Maeda, T. Takata, M. Hara, N. Saito, Y. Inoue, H. Kobayashi, K. Domen, J. Am. Chem. Soc. 127 (2005) 8286.
[11] K. Maeda, K. Teramura, T. Takata, M. Hara, N. Saito, K. Toda, Y. Inoue, H. Kobayashi, K. Domen, J. Phys. Chem. B 109 (2005) 20504.
[12] X. Sun, K. Maeda, M. Le Faucheur, K. Teramura, K. Domen, Appl. Catal. A Gen. 327 (2007) 114.
[13] K. Maeda, K. Teramura, D. Lu, T. Takata, N. Saito, Y. Inoue, K. Domen, Nature 440 (2006) 295.
[14] K. Maeda, K. Teramura, N. Saito, Y. Inoue, K. Domen, J. Catal. 243 (2006) 303.
[15] K. Maeda, K. Teramura, D. Lu, T. Takata, N. Saito, Y. Inoue, K. Domen, J. Phys. Chem. B 110 (2006) 13753.
[16] K. Maeda, K. Teramura, D. Lu, N. Saito, Y. Inoue, K. Domen, Angew. Chem. Int. Ed. 45 (2006) 7806.
[17] K. Maeda, K. Teramura, D. Lu, N. Saito, Y. Inoue, K. Domen, J. Phys. Chem. C 111 (2007) 7554.
[18] K. Maeda, K. Teramura, H. Masuda, T. Takata, N. Saito, Y. Inoue, K. Domen, J. Phys. Chem. B 110 (2006) 13107.
[19] M. Yashima, K. Maeda, K. Teramura, T. Takata, K. Domen, Chem. Phys. Lett. 416 (2005) 225.
[20] J. Shi, J. Chen, Z. Feng, T. Chen, Y. Lian, X. Wang, C. Li, J. Phys. Chem. C 111 (2007) 693.
[21] K. Maeda, K. Teramura, N. Saito, Y. Inoue, K. Domen, Bull. Chem. Soc. Jpn. 80 (2007) 1004.
[22] L. Jing, B. Xin, F. Yuan, L. Xue, B. Wang, H. Fu, J. Phys. Chem. B 110 (2006) 17860.
[23] T. Yoshihara, R. Katoh, A. Furube, Y. Tamaki, M. Murai, K. Hara, S. Murata, H. Arakawa, M. Tachiya, J. Phys. Chem. B 108 (2004) 3817.
[24] Y. Tamaki, A. Furube, M. Murai, K. Hara, R. Katoh, M. Tachiya, Phys. Chem. Chem. Phys. 9 (2007) 1453.
[25] N. Murakami, O.O.P. Mahaney, T. Torimoto, B. Ohtani, Chem. Phys. Lett. 426 (2006) 204.
[26] N. Murakami, O.O.P. Mahaney, R. Abe, T. Torimoto, B. Ohtani, J. Phys. Chem. C 111 (2007) 11927.